An Intelligent Speckle Reduction Algorithm for Optical Coherence Tomography Images

Saba Adabi[1,2], Silvia Conforto[2], Anne Clayton[1], Adrian G. Podoleanu[3], Ali Hojjat[4] and Mohammad R. N. Avanaki[1]

[1]*Wayne State University, Department of Biomedical Engineering, 818W Hancock St, Detroit, U.S.A.*
[2]*Roma Tre University, Department of Applied Electronics, Via V. Volterra 62, Rome, Italy*
[3]*University of Kent, Applied Optics Group, CT2 7PD, Canterbury, U.K.*
[4]*University of Kent, School of Physical Sciences, CT2 7NH, Canterbury, U.K.*

Keywords: Optical Coherence Tomography, Multi-Layer Perceptron (MLP), Speckle Noise Reduction, Artificial Neural Network (ANN).

Abstract: Optical Coherence Tomography (OCT) offers three dimensional images of tissue microstructures. Although OCT imaging offers a promising high resolution method, due to the low coherent light source used in the configuration of OCT, OCT images suffers from an artefact called, speckle. Speckle deteriorates the image quality and effects image analysis algorithm such as segmentation and pattern recognition. We present a novel and intelligent speckle reduction algorithm to reduce speckle based on an ensemble framework of Multi-Layer Perceptron (MLP) neural networks. We tested the algorithm on images of retina obtained from a spectrometer-based Fourier-domain OCT system operating at 890 nm, and observed considerable improvement in the signal-to-noise ratio and contrast of the images.

1 INTRODUCTION

Optical coherence tomography (OCT) is an advanced high resolution, non-invasive imaging modality which can be used to deliver three-dimensional (3D) images from microstructures within a tissue. As with other imaging modalities that employ coherent detection, OCT images are confounded by speckle (Podoleanu, 2014) (Goodman, 2007). In an optical imaging system, speckle imposes a grainy texture on images and decreases their signal-to-noise ratio (SNR) and their contrast-to-noise ratio (CNR). Consequently, speckle reduces the performance of image segmentation and pattern recognition algorithms that are used to extract, analyse, and recognize diagnostically relevant features. Development of successful speckle noise reduction algorithms for OCT is particularly challenging. The reason is that OCT speckle also carries structural information about the imaged object. A number of speckle reduction methods for OCT images have been developed using hardware modifications such as frequency compounding, shifting the focal plane of the probe beam, and angular compounding (Shankar, 1986) (Avanaki et al., 2013b). Besides the hardware modifications, a number of image processing algorithms have been reported such as adaptive digital filters, filters based on interval type II fuzzy algorithm, wavelet transformation with various configurations, or the use of median, averaging, Kuwahara filters and their combinations (Goodman, 2007) (Ozcan et al., 2007). We previously introduced an artificial neural network based (ANN) method for speckle reduction (Avanaki et al., 2008, Avanaki et al., 2013a). In that study, we modelled the speckle using a Rayleigh distribution with a single noise parameter, sigma, for the entire image. This parameter is estimated by the ANN. The algorithm was tested successfully on OCT images of Drosophila larvae, however we think it has the potential to have better efficiency. In this paper, we present a new scheme, in which the image is segmented into several sections. We also use a new ensemble framework which is a combination of networks. The noise parameter is then estimated using the MLP neural networks for different segments. Using these steps and a numerical method, the segments, and consequently the image is denoised. Further

Adabi, S., Conforto, S., Clayton, A., Podoleanu, A., Hojjat, A. and Avanaki, M.
An Intelligent Speckle Reduction Algorithm for Optical Coherence Tomography Images.
DOI: 10.5220/0005744700380043
In *Proceedings of the 4th International Conference on Photonics, Optics and Laser Technology (PHOTOPTICS 2016)*, pages 40-45
ISBN: 978-989-758-174-8

processing was performed to eliminate the blocking artefact.

2 METHODOLOGY

2.1 OCT Image Acquisition

The spectrometer-based Fourier-domain OCT system used to generate the retinal images is schematically presented in figure 1. Light from a low coherence source (two spectrally-shifted super-luminescent diodes (SLDs), with a central wavelength $\lambda_0 = 890$ nm and linewidth $\Delta\lambda = 150$ nm – Superlum Broadlighter D890) is directed to the two interferometer's arms via a fiber-based directional coupler (FDC). The object arm comprises a galvo-scanning mirror (SX) and an f-2f-f lens arrangement specifically devised for retinal imaging.

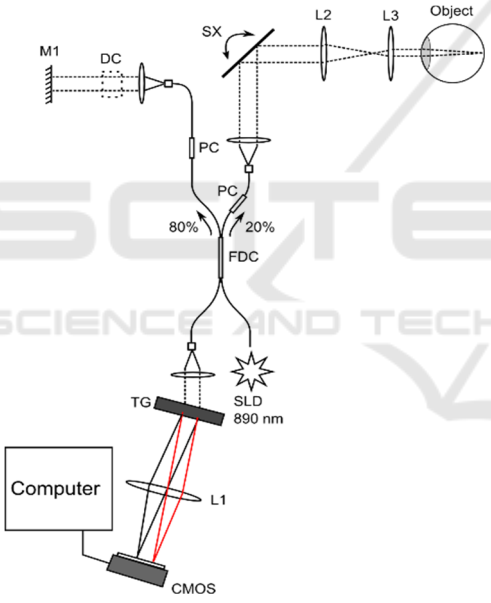

Figure 1: Spectrometer-based Fourier-domain optical coherence tomography system. SLD: super-luminescent diode with a central wavelength λ0 = 890 nm and linewidth Δλ = 150 nm, L1-L3: Achromatic Lenses, CMOS: Linear pixel array (line camera), SX: galvo-scanning mirror, TG: diffraction grating, M1: flat mirror, PC: polarization controller, FDC: 80/20 fused fiber directional coupler, DC: dispersion compensating element.

2.2 Speckle Reduction Algorithm

The algorithm we propose is composed of two phases. The first phase is the training phase. Using a Rayleigh noisy image generator in MATLAB, 10×10 pixels images were generated with sigma values (the single noise parameter employed in the Rayleigh function) ranging from 0 to 255 in steps of 0.05. For each sigma value, this procedure was repeated 100 times to generate numerous noisy images for training.

Three features - average, standard deviation, and median - were calculated from each segment and its wavelet sub-bands for training. Wavelet sub-band images were used to calculate the frequency domain statistical knowledge of the image. The neural network used is a combination of several MLP neural networks. The flow chart of algorithm is given in figure.2. Three MLP networks and a combiner, which is responsible for the averaging process, are the main components of this framework. Each of the MLP networks is composed of 15 neurons in its input layer, 10 neurons in its hidden layer and one output neuron to estimate the sigma parameter. The combiner is responsible for averaging with L neurons in input layer, L neurons in hidden layer and one output neuron which can estimate the sigma parameter in an ensemble fashion (in this paper, $L = 3$). To show the advantage of ensemble method over individual neural networks, let us consider a number of trained MLP neural networks L with outputs $y_i(\underline{x})$ (where x is an input vector). These estimate the sigma values using the i^{th} MLP neural network with an error of e_i with respect to the desired value of the sigma parameter, $h(\underline{x})$. In this situation, the following equation can be written as:

$$y_i(\underline{x}) = h(\underline{x}) + e_i \tag{1}$$

Thus the sum of squared error for the network y_i can be calculated using eq. (2):

$$E_i = \xi\left[\left(y_i(\underline{x}) - h(\underline{x})\right)^2\right] = \xi[{e_i}^2] \tag{2}$$

where $\xi[.]$ denotes the expectation (average or mean value). Thus the average error for the MLP networks acting individually can be calculated by eq. (3).

$$E_{AV} = \frac{1}{L}\sum_{i=1}^{L} E_i = \frac{1}{L}\sum_{i=1}^{L} \xi[{e_i}^2] \tag{3}$$

By averaging the outputs y_i, the committee prediction is obtained. This estimate will have an error equal to (eq. (4)):

$$E_{COM} = (y_{COM}(\underline{x}) - h(\underline{x}))^2 = \left[\left(\frac{1}{L}\sum_{i=1}^{L} y_i(\underline{x}) - h(\underline{x})\right)^2\right] = \xi\left[\left(\frac{1}{L}\sum_{i=1}^{L}[e_i]\right)^2\right] \tag{4}$$

Thus, using the Cauchy's inequality which is shown in eq. (5), one can show that $E_{COM} \leq E_{AV}$.

$$E_{COM} = \xi\left[\left(\frac{1}{L}\sum_{i=1}^{L}[e_i]\right)^2\right] \leq \frac{1}{L}\sum_{i=1}^{L}\xi[{e_i}^2] = E_{AV} \quad (5)$$

The neural network delivered the highest reliability in the estimation of the sigma value when a Daubechies 4 (db4) mother function was used. There are a total of 12 inputs to the neural network. The transfer function, performance function, learning function, network size, and number of hidden layers, were chosen experimentally such that optimum network reliability is achieved. Such reliability is defined as the percentage ratio of the difference between the expected sigma value and the estimated sigma over the expected sigma value. The averaged reliability of the sigma estimator network measured over 20 runs was 99.3 percent that was greater than our previous ANN that had a reliability of 98.8 percent. The second phase is the testing phase. As shown in the de-speckling flowchart in figure 2, the OCT image is initially divided into several segments based on the homogeneity. Similar to the training stage, the same pre-processing was applied to each image, and then the statistical features were extracted from each segment in the image and used as input for the neural network. The Rayleigh noise parameter was then estimated for each segment using the trained network (Avanaki and Hojjatoleslami, 2009). The estimated sigma is then used along with a numerical method to solve the inverse Rayleigh function numerically for each segment. Putting together the noise model segments, we can generate a noise model image. The noise model image was deducted from the original image with a scale factor which was obtained experimentally. To remove the blocking artifact, following the method given in (Fitzpatrick, 1975), some statistical features were extracted from the original image, based upon which of the despeckled segments are then stitched together.

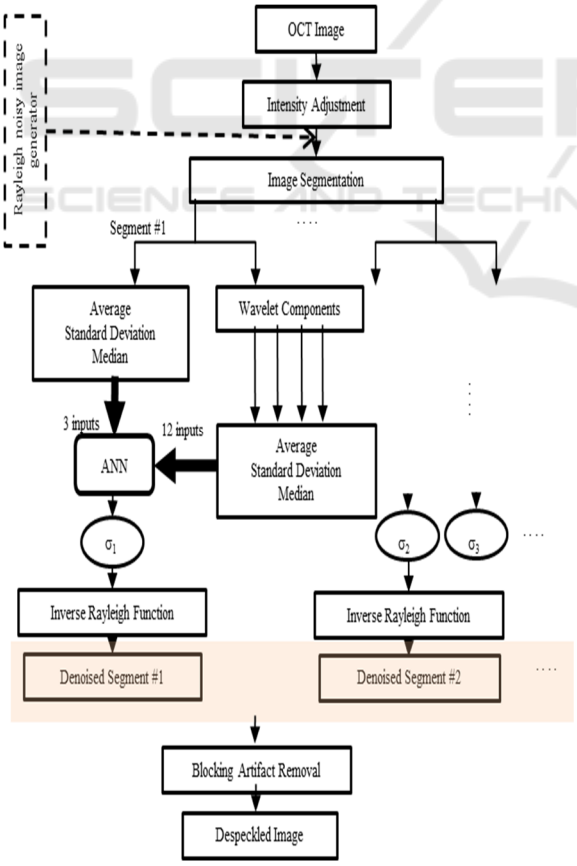

Figure 2: Schematic diagram of the despeckling algorithm. The blocks in the dotted box are used in the training phase.

3 RESULTS AND DISCUSSION

B-scan OCT images of eye (*in-vivo*) were used to test the algorithm. The OCT images before and after de-speckling algorithm are shown in figure 3. The number of segments in each image affects the despeckling efficiency. To improve edge sharpness and have more effective blocking artifact removal, we segment our images into eight sub images. The estimated sigma values for the segments within the images are given in table 1, table 2 and table 3 corresponded to figure. 3, figure.4, figure.5 respectively.

Table 1: The estimated sigma values for figure. 3, The number of segments are 8 (4 segments in each row).

Segment #	Sigma
1	112
2	56
3	21
4	41
5	131
6	145
7	162
8	143

To evaluate the improvement of the images after de-speckling, we calculated the signal-to-noise ratio and the contrast-to-noise ratio (CNR) as defined in eq. (6) and eq.(7) respectively (Shankar, 1986).

$$SNR = 10\log_{10}\left(\frac{(\max I)^2}{\sigma_b{}^2}\right) \quad (6)$$

$$CNR = \frac{1}{R}\left(\sum_{r=1}^{R}\frac{(\mu_r - \mu_b)}{\sqrt{\sigma_r{}^2 + \sigma_b{}^2}}\right) \quad (7)$$

where $\max(I^2)$ represents the maximum of squared intensity pixel values in a homogeneous region of interest in the linear magnitude image, where μ_b and $\sigma_b{}^2$ and CNR represents the mean, variance of the same background noise region, and μ_r and $\sigma_r{}^2$ represents the mean and variance of the R region of interest (Shankar, 1986).

Table 2: The estimated sigma values for figure. 4, The number of segments are 8 (4 segments in each row).

Segment #	Sigma
1	98
2	64
3	51
4	45
5	68
6	20
7	39
8	81

Table 3: The estimated sigma values for figure. 5, The number of segments are 8 (4 segments in each row).

Segment #	Sigma
1	75
2	64
3	56
4	68
5	28
6	30
7	27
8	19

In-line with other published work (Shankar, 1986), we used 5 regions (R=5) in the calculation of CNR. The results of these calculations on three test images are given in Table 2. We compared the performance of the proposed method in this article with some other existing methods (see figure 3, figure 4 ad figure 5). We observed a blurring artifact in the averaged image, as well as in the median filtered image that was not observed in the denoised image using our proposed method. It was also perceived that the median filtered image is more pronounced in terms of image contrast. The quantitative assessments of the despeckled image showed in figure.3, figure.4 and figure.5 demonstrated that the proposed method can provide an extra enhancement.

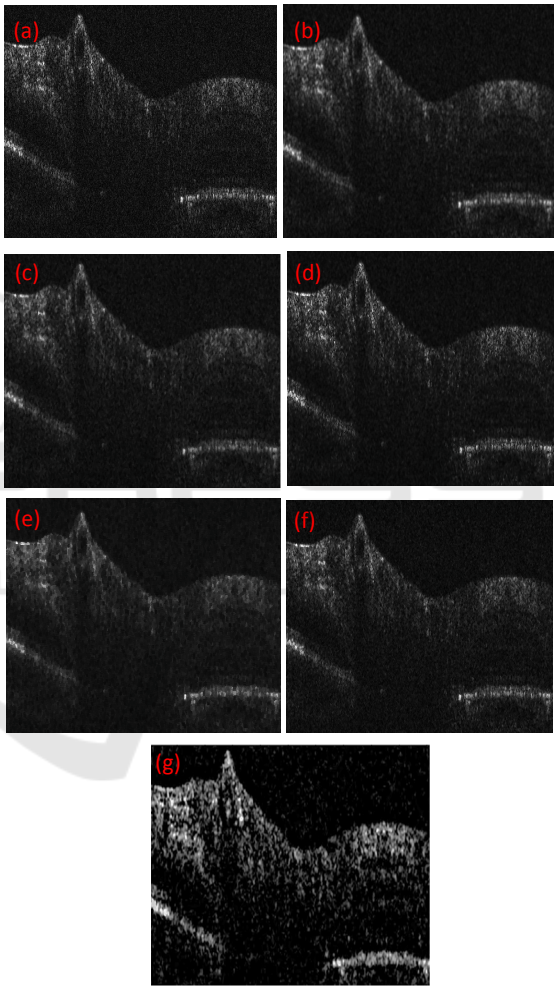

Figure 3: Comparative presentation of six despeckling methods on an original OCT test images acquired from the retina (optic nerve region) of a volunteer (AP), white male, provided by Adrian Podoleanu's lab. (a) Original B-scan image of optic nerve, lateral size ~ 1-1.2 mm, (b) the B-scan image after average filtering (window size: 3), (c) the B-scan image after median filtering (window size: 3), (d), the B-scan image after wiener filtering (window size: 3), (e) the B-scan image after Kuwahara filtering (window size: 5), (f) the B-scan image after SNN filtering (window size: 3), (g) the B-scan image after using the proposed method.

of around 8 dB and 0.6 in terms of SNR and CNR respectively compared to their counterparts in averaging and median filtering Moreover, the proposed method surpassed both Symmetric Nearest Neighbourhood and Winner noise reduction filters by increment of around 3dB in terms of SNR. However in case of CNR a difference of 0.2 is observed. Kuwahara filtered image has a SNR of 4dB and CNR of 0.1 less than filtered image using proposed method is depicted in figure.6. It should be noted that this fast real-time effective algorithm could be enhanced by utilizing a more accurate estimation of sigma employing an improved version of ANN and using a more precise valuation of noise model mathematically. Moreover a possible improvement can be achieved referring to image segments. A future study planned to cover those issues.

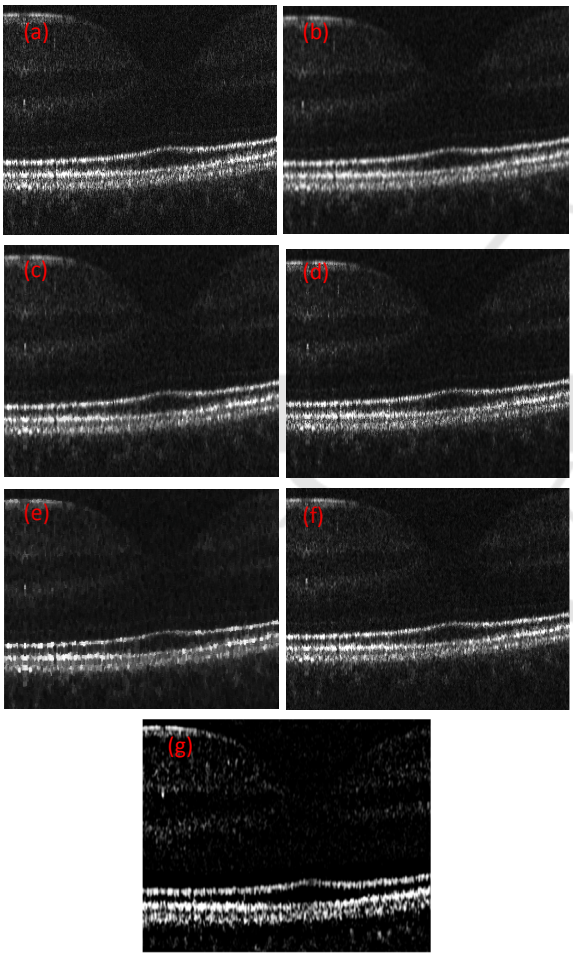

Figure 4: Comparative presentation of six despeckling methods on an original OCT test images acquired from the retina (optic nerve region) of a volunteer (AB-fovea), white male (a) Original B-scan image of optic nerve,(b) the B-scan image after average filtering (window size: 3), (c) the B-scan image after median filtering (window size: 3), (d) the B-scan image after wiener filtering (window size: 3), (e) the B-scan image after Kuwahara filtering (window size: 5), (f) the B-scan image after SNN filtering (window size: 3), (g) the B-scan image after using the proposed method.

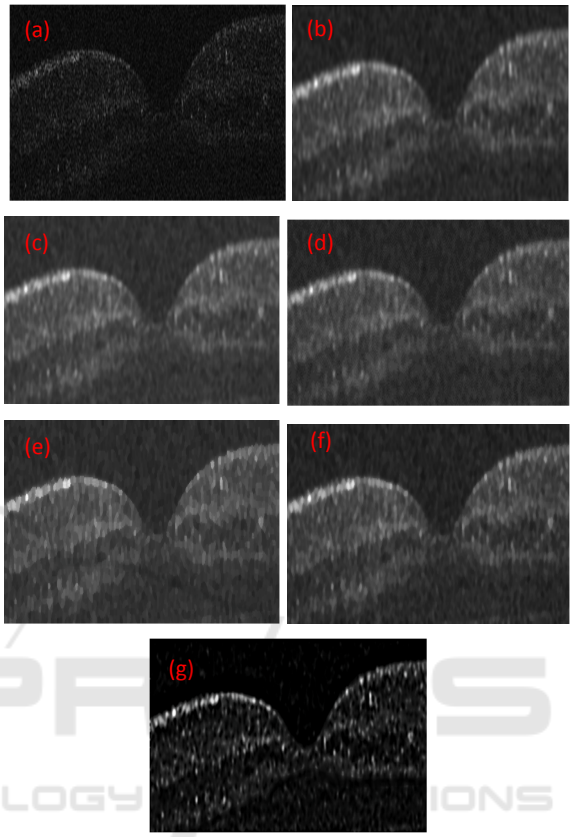

Figure 5: Comparative presentation of six despeckling methods on an original OCT test images acquired from the retina (optic nerve region) of a volunteer (AB-fovea), white male (a) Original B-scan image of optic nerve, (b) the B-scan image after average filtering (window size: 3), (c) the B-scan image after median filtering (window size: 3), (d) the B-scan image after wiener filtering (window size: 3), (e) the B-scan image after Kuwahara filtering (window size: 5), (f) the B-scan image after SNN filtering (window size: 3), (g) the B-scan image after using the proposed method. The vertical axis is z-axis.

Table 4: Numerical assessment of the proposed denoising algorithm using SNR and CNR metrics.

	SNR		CNR	
	Original	Despeckled	Original	Despeckled
(I1)	9.2	26	2.5	4
(I2)	12.1	31	3	5.9
(I3)	11.5	24	1.9	3.2

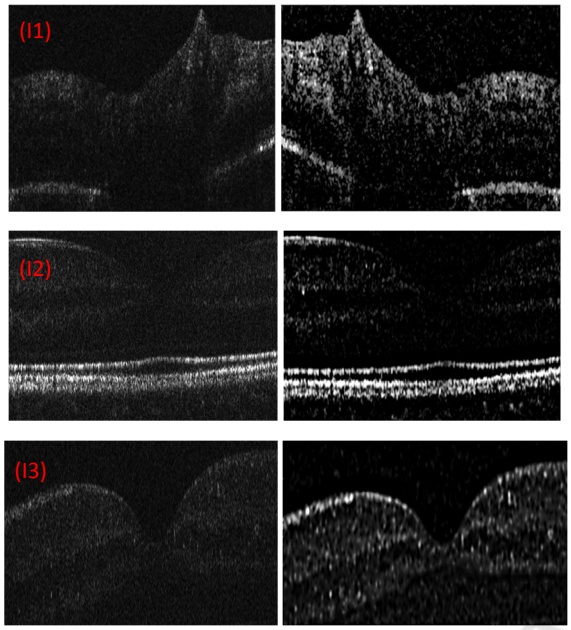

Figure 6: Comparative presentation of three original OCT test images (I1), (I2), (I3) and of their denoised images.

4 CONCLUSIONS

In this paper, a speckle reduction algorithm was presented based on the approximation that speckle noise has a Rayleigh distribution with a noise parameter, sigma. A new ensemble framework as a combination of several Multi-Layer Perceptron (MLP) neural networks was designed to estimate sigma in the speckle noise model. The sigma estimator kernel worked with more than 99.3% reliability on average. The estimated sigma values were then used in the de-speckling algorithm to reduce the speckle in the OCT images. The algorithm was successful in reducing speckle of B-scan images of human eye. The algorithm reduced the speckle while preserved the details of the regions. Two well-established no-reference quality metrics including SNR and CNR were used for quantitative evaluation, and demonstrated higher quality images when the new algorithm was utilized. The proposed algorithm is also compared with some other bilateral digital filters and demonstrated a satisfying evaluation. Respectively, due to the generality of proposed ANN algorithm, it can be used as a signal processing method in other image modalities such as photoacoustic imaging system (Nasiriavanaki et al., 2014).

REFERENCES

Avanaki, M., Laissue, P. P., Eom, T. J., Podoleanu, A. G. & Hojjatoleslami, A. 2013a. Speckle reduction using an artificial neural network algorithm. *Applied optics,* 52**,** 5050-5057.

Avanki, M. R., Cernat, R., Tadrous, P. J., Tatla, T., Podoleanu, A. G. & Hojjatoleslami S. A. 2013b. Spatial compounding algorithm for speckle reduction of dynamic focus OCT images. *Photonics Technology Letters, IEEE,* 25**,** 1439-1442.

Avanaki, M. R. & Hojjatoleslami, A. 2009. Speckle reduction with attenuation compensation for skin OCT images enhancement. *Proceeding of Medical Image Understanding and Analysis (MIUA), Kingston University, London***,** 14-15.

Avanaki, M. R., Laissue, P. P., Podoleanu, A. G. & Hojat, A. Denoising based on noise parameter estimation in speckled OCT images using neural network. 1st Canterbury Workshop and School in Optical Coherence Tomography and Adaptive Optics, 2008. International Society for Optics and Photonics, 71390E-71390E-9.

Fitzpatrick, T. B. 1975. Soleil et peau. *J Med Esthet,* 2**,** 33-34.

Goodman, J. W. 2007. *Speckle phenomena in optics: theory and applications*, Roberts and Company Publishers.

Nasiriavanaki, M.R.N, Xia, J., Wan, H., Bauer, A. Q., Culver, J. P. & Wang, L. V. 2014. High-resolution photoacoustic tomography of resting-state functional connectivity in the mouse brain. *Proceedings of the National Academy of Sciences,* 111**,** 21-26.

Ozcan, A., Bilenca, A., Desjardins, A. E., Bouma, B. E. & Tearney, G. J. 2007. Speckle reduction in optical coherence tomography images using digital filtering. *JOSA A,* 24**,** 1901-1910.

Podoleanu, A. G. 2014. Optical coherence tomography. *The British journal of radiology*.

Shankar, P. M. 1986. Speckle reduction in ultrasound B-scans using weighted averaging in spatial compounding. *IEEE transactions on ultrasonics, ferroelectrics, and frequency control,* 33**,** 754-758.